J Mater Sci: Mater Electron (2017) 28:16696–16703
DOI 10.1007/s10854-017-7582-2

Synthesis of graphene oxide/Ag_3PO_4 composite with enhanced visible-light photocatalytic activity

Qishe Yan[1] · Xin Xie[1] · Cuiping Lin[1] · Yalei Zhao[1] · Shenbo Wang[1] · Yonggang Liu[1]

Received: 13 May 2017 / Accepted: 20 July 2017 / Published online: 24 July 2017

Abstract The nano-scale Ag_3PO_4 was successfully synthesized by the silver ammonia complexing precipitation method at room temperature. And the Graphene oxide (GO)/Ag_3PO_4 nanocomposites with different contents of GO were successfully synthesized using the electrostatic driving method. The as-prepared GO/Ag_3PO_4 nanocomposites were characterized by X-ray diffraction (XRD), scanning electron microscopy (SEM), and UV–visible diffuse reflectance spectroscopy (UV–Vis DRS), confirming that Ag_3PO_4 were highly dispersed to GO sheet. The photocatalytic properties of GO/Ag_3PO_4 were evaluated by the degradation of Methyl Orange (MO) under visible light irradiation and solar irradiation respectively. The results showed that the photocatalytic efficiencies of GO/Ag_3PO_4 nanocomposites had enhanced largely and the kinetics reaction models were followed first-order. Furthermore, 5% GO/Ag_3PO_4 exhibited the highest photocatalytic activity on degradation of MO under visible-light irradiation. The improved photocatalytic performances of the GO/Ag_3PO_4 nanocomposites mainly attributed to the introducing of GO, which benefit for electron transfer and inhibit the recombination of electron–hole pairs, promoting the practical application of Ag_3PO_4 in water purification.

1 Introduction

Since the 1970s, environment pollution has gradually become a global problem, especially the water pollution results from the massive discharge of industrial wastewater, such as dyeing and printing wastewater [1]. Those toxic and cancerogenic pollutants threaten human health seriously. Therefore, developing security and efficient technology to control environmental pollution become the most urgent task [2]. Among that, semiconductor photocatalyst is considered to be one of the most promising technologies to degrade organic pollutants from wastewater since the utilization of solar energy, which is inexhaustible clean and security [3]. As early as 1972, Fujishima and Honda discovered the photocatalytic properties of TiO_2 electrode for the first time, which is known as a milestone in the process of photocatalysis research [4]. Although TiO_2 has the advantages of high photocatalytic activity, chemical stability, non-toxic and low cost [5–7], it can only utilize the ultraviolet light which account for 5% of the sunlight due to a wide band gap of 3.2 eV [8, 9]. Furthermore, the low separation and high recombination rate of the photoexcited electron–hole in TiO_2 seriously limit its quantum efficiency [10]. Therefore, exploring new active and efficient visible light-responsive photocatalyst still remains a challenge.

As an efficient photocatalytic material for water photooxidation and organic dye photodecomposition under visible light irradiation, visible-light-driven photocatalysts silver orthophosphate (Ag_3PO_4) has been attracted many attentions since it was firstly discovered by Ye and co authors [11]. The band gap of Ag_3PO_4 is 2.36 eV which is much sharper than TiO_2, that is to say, Ag_3PO_4 can make full use of the solar energy [12]. Furthermore, Ag_3PO_4 has extremely high quantum efficiency, low toxicity and high photocatalytic activity [13, 14], leading to a superior photocatalytic performance than well-studied visible-driven photocatalyst, such as $BiVO_4$ and WO_3 [15, 16]. However, there are also some limitations in the Ag_3PO_4 photocatalyst system, especially the stability. On the one hand, the

✉ Qishe Yan
Qisheyanzzu@163.com

[1] College of Chemistry and Molecular Engineering, Zhengzhou University, Zhengzhou 450001, China

structural stability of Ag_3PO_4 is a little poor as Ag_3PO_4 is slightly soluble in aqueous solution [17]. On the other hand, Ag_3PO_4 has a serious photocorrosion phenomenon that the interstitial silver ion (Ag^+) in aqueous solution invariably combines with the photogenerated electron and transform into silver atom (Ag) during the photocatalytic process, which results in a poor chemical stability of Ag_3PO_4 [18]. Although sacrificial reagents such as $AgNO_3$ can provide electron acceptor and reduce the photocorrosion [19], it would increase the amount of noble Ag and to a certain extent increase the cost. Furthermore, the metallic Ag particles in the reaction systems would load on the surface of the Ag_3PO_4 photocatalytic, which would restrain the absorption of Ag_3PO_4 and then decrease the photocatalytic activity [20]. Therefore, it is of great necessary to further develop new Ag_3PO_4-based photocatalysts with good stability, efficient charges separation, high photocatalytic activity and low cost.

There are many efforts have been done on modification of Ag_3PO_4 by introducing various photocatalytically active components such as WS_2/Ag_3PO_4 [21], $CoFe_2O_4/Ag_3PO_4$ [22], CNT/Ag_3PO_4 [23], $P/Ag/Ag_2O/Ag_3PO_4/TiO_2$ [24] and so on. Among them, GO has received increasing attentions in recent years on photodegradation of organic contaminants in wastewater due to its remarkable photocatalytic properties [25–27]. GO is a monolayer two-dimensional (2D) planar honeycomb lattice made of hexagonally arrayed sp^2-bonded carbon atoms [28], with a thickness of 0.335 nm, a large specific surface area of 2630 m^2/g, a good thermal conductivity properties of 3000 W/(m K) and an excellent electrical conductivity [29]. Apart from the excellent electronic properties, GO has a good chemical stability and carrier mobility [30]. Because of the superior photocatalytic properties, GO has been widely used as a carrier compositing with other photocatalysts, such as ZrO_2/GO [31], C_3N_4/GO [32], and $Ag/AgCl/GO/Fe_3O_4$ [33]. These studies found that the photocatalytic performance of GO-based hybrid photocatalyst composites is extraordinarily enhanced in the photodegradation of organic contaminants mainly because the GO sheets act as a electron sink and transfer bridge to accelerate the transfer and reduce the recombination of electron–hole pairs, so as to improve the photoconversion efficiency and stability of photocatalysts by decreasing their photocorrosion [34]. Besides, GO can facilitate the contaminants adsorbing on the photocatalysts and extend its light absorption range [35]. Therefore, in consideration of the superior properties of GO and the limitation of Ag_3PO_4, the combination of GO and Ag_3PO_4 is a promising strategy to develop a stable and efficient photocatalyst composite. Although many works have been done in this part [36, 37], most of the as-synthesized Ag_3PO_4/GO composites were spherical and of micro-scale [13], which severely restricted its photocatalytic performance, and finding a method for better morphology and smaller size of Ag_3PO_4 is still need a further study.

Herein, nano-scale Ag_3PO_4 photocatalyst was fabricated with the adding of PVP and ammonia, which can control the release of Ag^+ effectively to reduce the rate of generation of Ag_3PO_4, achieving the purpose of controlling the morphology, and then associated with GO using the electrostatic driving method. The structure characterizations demonstrated that Ag_3PO_4 is successfully attached on GO. The introducing of GO had greatly improved the photocatalytic properties of pure Ag_3PO_4, and the obtained Ag_3PO_4/GO composite photocatalys exhibited an excellent photocatalytic activity and stability on degradation of Methyl Orange (MO) in aqueous solution under visible-light irradiation. Furthermore, it is investigated that the introducing of GO seriously affects the photocatalytic activity of Ag_3PO_4 and the increasing content of GO effectively enhances the photocatalytic performance of the as-prepared Ag_3PO_4/GO composite photocatalys. These composite photocatalys provide Ag_3PO_4 a possibility of practical application.

2 Experimental

2.1 Reagents

All reagents were of analytical pure and were used as received without further purification. Natural graphite powder (99.95%) was purchased from Shanghai Aladdin Bio-Chem. Tech. Co., Ltd. Concentrated sulfuric acid (H_2SO_4) and hydrochloric acid (HCl) was purchased from Luoyang Hao Hua Chem. Reagent Factory. Potassium hypermanganate ($KMnO_4$) was purchased from Beijing Hua Teng Chem. Reagent Co., Ltd. Hydrogen peroxide (H_2O_2) was purchased from Sinopharm Chemical Reagent Co., Ltd. Silver nitrate ($AgNO_3$) and disodium hydrogen phosphate dodecahydrate ($Na_2HPO_4\cdots12H_2O$) were purchased from Tianjin Kermel Chem. Reagent Co., Ltd. Absolute ethyl alcohol (CH_3CH_2OH) was purchased from Tianjin Fuchen Chem. Reagent Co., Ltd. Methyl orange (MO) was purchased from Shanghai Chemical Dispensing Factory.

2.2 Synthesis of GO

GO was synthesized by strong oxidant $KMnO_4$ using modified Hummers method. First, 98% concentrated H_2SO_4 (70 mL), 1.0 g of graphite powder and 1.5 g of $NaNO_3$ was successively added into a 1000 mL flask under the condition of vigorous stirring and ice bath (below 20 °C). Keeping the temperature below 4 °C, $KMnO_4$ (9.0 g) was added gradually until the solution transformed to emerald green. And then, the flask was transferred to the oil bath pot controlling the temperature at around 40 °C with magnetic

stirring 40 min. 150 mL of distilled water was slowly added to the reaction mixture, in this process the temperature was up to 95 °C. After heating for 15 min, the solution transformed to brown and the flask was removed out of the oil bath pot. After the slow adding of 500 mL distilled water, 30% H_2O_2 (30 mL) was added dropwise to the solution and then stopt stirring and heating when the system became brilliant yellow. The precipitate was obtained by centrifuged (4000 r/min, 10 min) and washed with HCl (1:10) and distilled water for three times respectively. The obtained GO was dialyzed for 2 weeks and changed water every day. After ultrasonic and centrifugal (4000 r/min) for 30 min, the precipitate (agglomerated GO) was removed and the supernatant was obtained. After ultrasonic and centrifugal again, the solution was divided into three layers, and the precipitate and supernatant was removed by a straw and the interlayer (small pieces of GO sheets) was obtained. Finally, the GO was calibrated as 0.01 g/mL.

2.3 Synthesis of GO/Ag_3PO_4

Using the PVP as a structure reducer, a series of GO/Ag_3PO_4 visible light response photocatalysts were synthesized by the silver ammonia complex precipitation method. First, 0.25 g PVP and 1.2 g $AgNO_3$ were successively added into 300 mL deionized water with continuous stirring. After 20 min magnetic stirring in darkness, Ammonia solution (1:1, v:v) was added drop-by-drop until the solution became clear and stirred for 10 min constantly. Then, 1, 5 and 10 mL GO solution was dispersed into the above solution and were designed as 1, 5, 10% Ag_3PO_4/GO respectively. During vigorous stirring for 6 h, the electrostatic driving force between positively charged Ag^+ and negatively charged GO sheets made Ag^+ anchored on the surface of GO efficiently [38]. 47.1 mL Na_2HPO_4 (0.3 M) solution was added dropwise to above mixture solution and stirred for 4 h. The filtered precipitate was washed with deionized water and absolute ethanol for three times respectively and dried at 70 °C for 12 h. And similar procedures were used to prepare pure Ag_3PO_4 without the presence of GO.

2.4 Characterization

The X-ray diffraction (XRD) analysis were carried out with an X-ray diffractometer (D/MAX-rA, Rigaku, Japan) equipped with a Cu Kα X-ray source and operated at a voltage of 50 kV and a current of 50 mA, in the 2θ range from 5° to 90° at a scanning step of 0.02°. The morphology of the samples was characterized by scanning electron microscopy (FE-SEM, Sigma 500, zeiss). UV–Vis diffuse reflection spectra (UV–Vis DRS) was performed by using a UV–Vis spectrophotometer (Caly 5000, Agilent, USA) and $BaSO_4$ was used as the reflectance. The band gap energy (E_g) can be obtained according to the equation:

$$\alpha(hv) = A(hv - E_g)^2$$

where α, $h\nu$, and A are the absorption coefficient, photo engrgy and a constant, respectively.

2.5 Photocatalytic experiments

The photocatalytic properties of GO/Ag_3PO_4 with different content of GO were investigated by the photodegradation of Methyl Orange (MO) under 300 W xenon lamp. First, photocatalyst (50 mg) was added into 50 mL of MO (20 mg/L) solution and stirred for 0.5 h in darkness to reach the adsorption and desorption equilibrium. Then the suspension was irradiated by visible-light using 300 W xenon lamp with constantly stirring. During irradiation, 2 mL solution were sampled at the given time intervals and filtered the catalyst. The concentration changes of MO can be measured by the maximum absorption wavelength of MO recorded by UV–Vis spectroscopy (UV-2450, Shimadzu, Japan).

3 Results and discussions

3.1 Characterization of photocatalysts

The XRD patterns of as-synthesized GO sheets and GO/Ag_3PO_4 composites obtained with initial GO content of 1, 5 and 10% were shown in Fig. 1. It is clear that the typical diffraction peak of GO was located at 10.9 °C indicating that G was oxidized to GO completely [39]. According to the Bragg equation: $2d\sin\theta = n\lambda$, it could be calculated that the thickness of GO was 0.75 nm corresponding to 0.8 nm which a paper has been reported before [40]. As for GO/Ag_3PO_4 composites, it is clear that all of the diffraction peaks could be indexed to Ag_3PO_4 (JCPDS card No. 06-0505) and no peak attributed to other phases was observed which indicated that Ag_3PO_4 was extremely pure. Furthermore, the diffraction peaks of the samples were strong and sharp demonstrating that Ag_3PO_4 had a high degree of crystallization. Because of the relatively low diffraction intensity of GO, there was no diffraction peak of GO appears in the XRD patterns of GO/Ag_3PO_4 composites, indicating that the introduction of the GO just influenced the diffraction intensity of Ag_3PO_4, rather than the structure of the peak.

The morphology structures of the as-synthesized GO, Ag_3PO_4 and GO/Ag_3PO_4 composites were observed by SEM (Fig. 2). The SEM image of pure Ag_3PO_4 was shown in Fig. 2a, b. The pure Ag_3PO_4 particles had an irregular

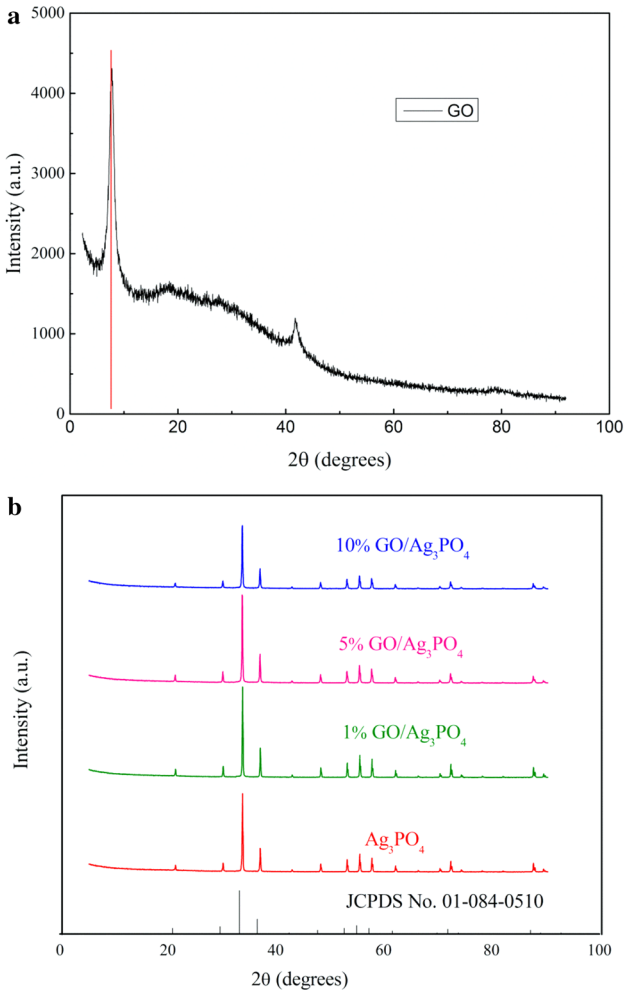

Fig. 1 XRD patterns of GO and GO/Ag_3PO_4 composites obtained with initial GO content of 1, 5, 10%

structure with the size of approximately 200–1000 nm, which was smaller than most of the as-synthesized Ag_3PO_4 [41]. And the small-sized Ag_3PO_4 may attribute to the addition of PVP and $NH_3{\cdot}H_2O$. Figure 2c shown the SEM images of GO. It could be observed that the gauze-like GO had a relatively big wrinkle surface, which would provide more active sites for Ag_3PO_4 to anchor on. Figure 2d–f shown the SEM images of GO/Ag_3PO_4 composites with GO content of 1, 5 and 10% respectively. It is clear that the irregular Ag_3PO_4 particles were wrapped by GO or randomly distributed on the surface of GO. This structure could prevent the agglomeration of Ag_3PO_4 and beneficial for the separation and transportation of electron–hole pairs, which were the key issues to improve the photocatalytic efficiency of degradation. Additionally, it could be observed from Fig. 2d that some of the Ag_3PO_4 particles were not anchored on the surface of GO due to the introduction amount of GO was relatively low. Conversely, Fig. 2f shown that the surface of GO was still available for more particles to anchored. And in the Fig. 2e, the Ag_3PO_4 particles adequately composited with GO insuring the sufficient contact between Ag_3PO_4 and GO, which may result in a better photodegradation performance.

The optical properties of GO, pure Ag_3PO_4, and GO/Ag_3PO_4 composites were investigated by UV–Vis DRS, and the UV–Vis spectrum were illustrated in Fig. 3. The result shown that all of the samples exhibited photoabsorption in the UV and visible region but had significant different absorptive intensity. It is obvious that pure Ag_3PO_4 shown the lowest absorption ability in the visible light, and with the increase of GO content in the sample, the absorption ability of GO/Ag_3PO_4 composites became stronger. Therefore, the as-synthesized GO/Ag_3PO_4 composites may have a higher utilization efficiency of sunlight, which was the key point in photocatalytic degradation. The optical absorption edge of pure Ag_3PO_4 was detected at around 533 nm corresponding to the paper reported before [11], and was not shifted in the spectrum of GO/Ag_3PO_4 composites indicating that carbon was free rather than incorporated to the Ag_3PO_4 [42].That is to say GO/Ag_3PO_4 composites had an intense and broad background absorption [43], which beneficial for better photocatalytic performance.

Band-gap energy of pure Ag_3PO_4 and GO/Ag_3PO_4 composites could be obtained according to the equation mentioned above, as shown in Fig. 4. The band gap energy of pure Ag_3PO_4 was calculated to be 2.3 eV which was considerable shorter than the band gap energy of TiO_2 (3–3.2 eV), indicating that the as-synthesized Ag_3PO_4 photocatalyst could utilize sunlight availably. Furthermore, with the increase of GO content in GO/Ag_3PO_4 composites, the band gap energy became shorter and shorter. The band gap energy of 1% GO/Ag_3PO_4 composites was estimate to be 2.2 eV while the values for 5 and 10% GO/Ag_3PO_4 composites wew fairly low. The narrow band gap meant that electron excited from valence band to conduction band become easier in consideration of the lower energy requirement which both ultraviolet light and visible light could meet. Namely, GO/Ag_3PO_4 composites exhibited better abilities to utilize sunlight and may have a better performance in photocatalytic degradation.

3.2 Photocatalytic activity

The photocatalytic behaviors of as-prepared GO/Ag_3PO_4 composites were investigated by the photodegradation of MO dye under visible-light and solar irradiation respectively.

Using C/C_0 as a function of irradiation time, Fig. 5 shown the photodegradation curves of MO over different photocatalysts under visible-light irradiation. It could be observed that with the increase of irradiation time, the

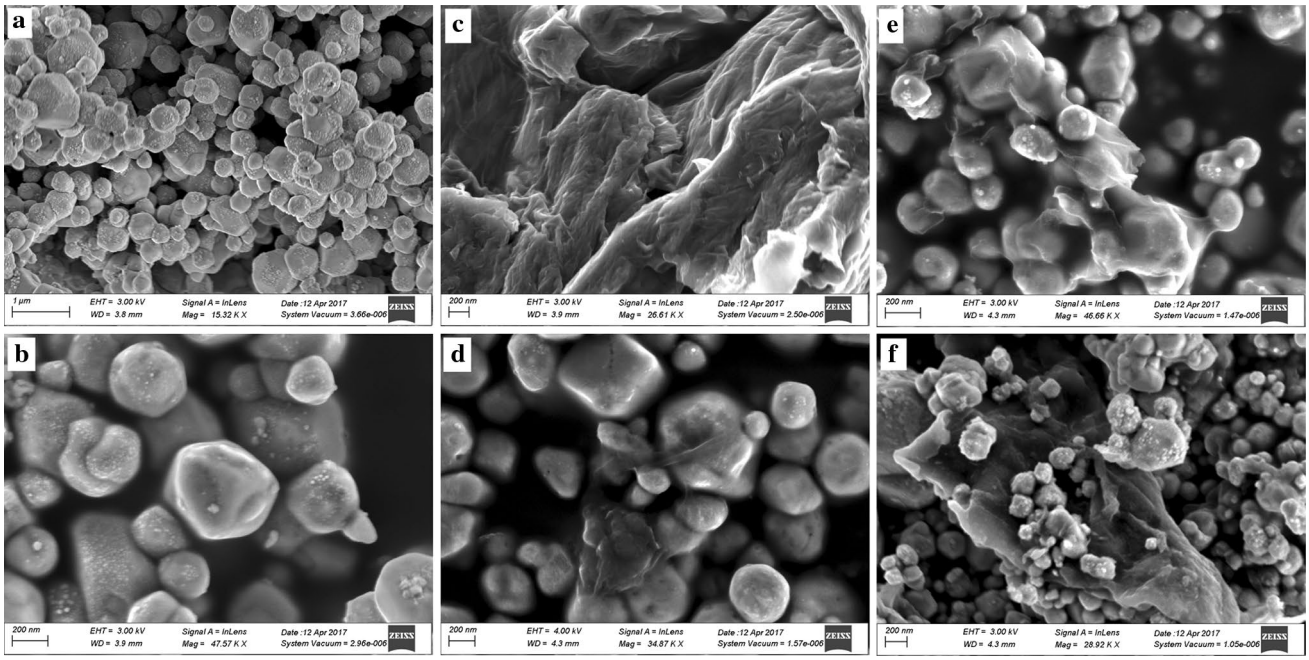

Fig. 2 SEM of samples: **a, b** Ag_3PO_4; **c** pure GO; **d** 1% GO/Ag_3PO_4 composites; **e** 5% GO/Ag_3PO_4 composites; **f** 10% GO/Ag_3PO_4 composites

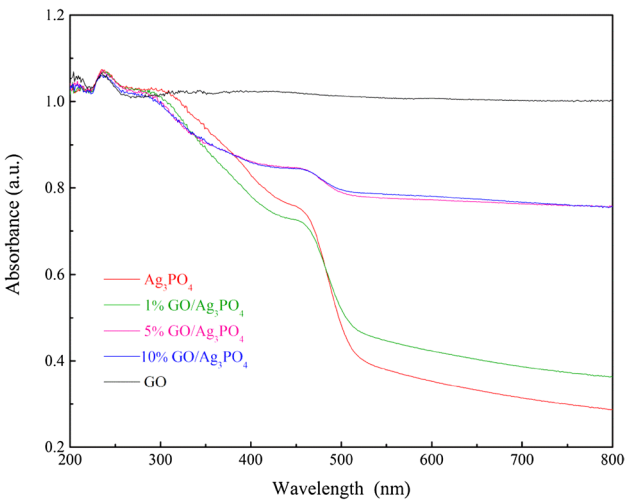

Fig. 3 UV–Vis DRS of GO, pure Ag_3PO_4 and GO/Ag_3PO_4 composites

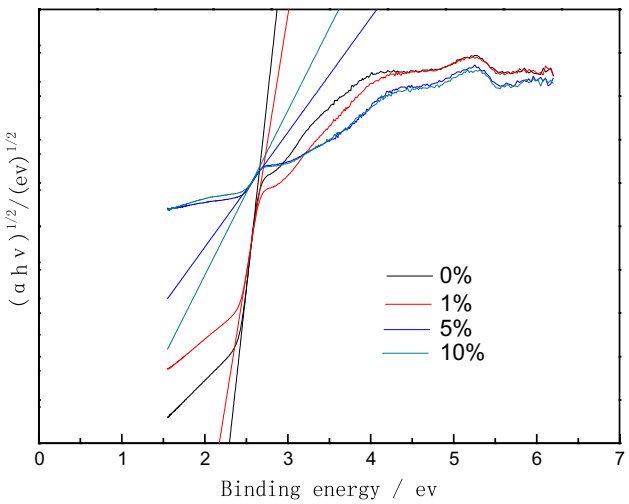

Fig. 4 Band-gap energy of pure Ag_3PO_4 and GO/Ag_3PO_4 composites

values of C/C_0 were reduced indicating that the concentrate of MO in the solution was gradually reduced, declaring that all of the samples possessed visible light responsive activities. Detailedly, after 60 min of irradiation, the decomposition ratio of pure Ag_3PO_4, 1, 5 and 10% GO/Ag_3PO_4 composites were 24, 52, 84 and 84% respectively. And after 120 min of irradiation, the decomposition ratio of pure Ag_3PO_4, 1, 5 and 10% GO/Ag_3PO_4 composites were 33, 58, 83 and 84% respectively. Results shown that the decomposition ratio was positive related to the initial contents of GO in the samples. It is noteworthy that the decomposition ratios of 5 and 10% GO/Ag_3PO_4 composites were extremely fast 30 min before and remain about the same 40 min after. Furthermore, 5 and 10% GO/Ag_3PO_4 composites exhibited superior photocatalytic activity while pure Ag_3PO_4 shown relatively low activity and 5% GO/Ag_3PO_4 composites possessed the highest degradation rate.

Figure 6 shown the photodegradation curves of MO over different photocatalysts under solar irradiation. After

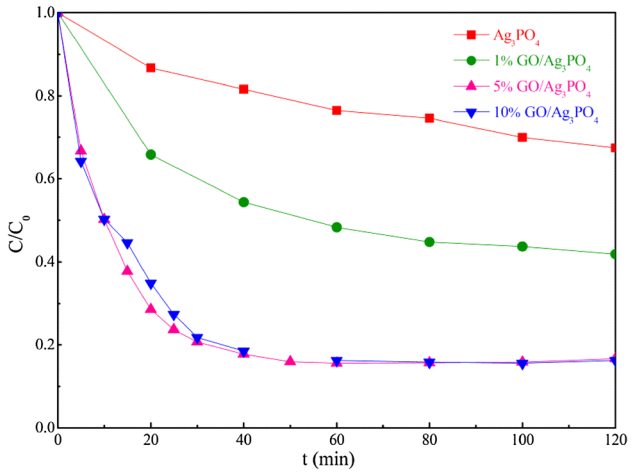

Fig. 5 Photocatalytic *curves* of MO using different photocatalysts under visible-light irradiation

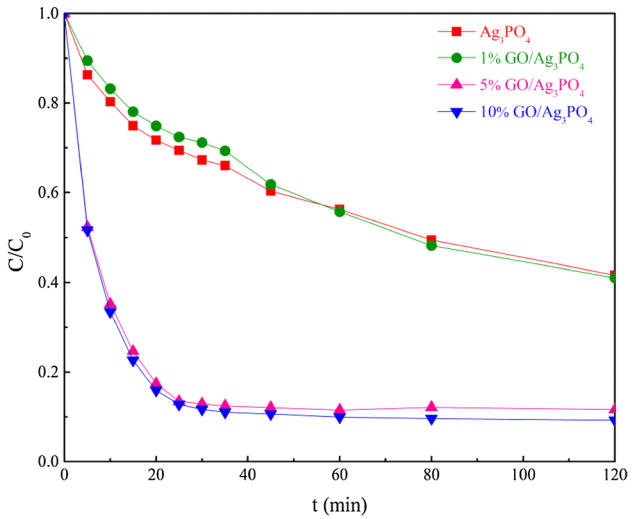

Fig. 6 Photocatalytic *curves* of MO using different photocatalysts under solar irradiation

60 min of irradiation, pure Ag_3PO_4 and 1% GO/Ag_3PO_4 composites only decomposed 44% of MO while 5 and 10% GO/Ag_3PO_4 composites had already decomposed 88 and 90% respectively. Then after 120 min of irradiation, 88 and 91% of MO were degraded in the presence of 5 and 10% GO/Ag_3PO_4 composites respectively, whereas only 58 and 59% of the MO were degraded for pure Ag_3PO_4 and 1% GO/Ag_3PO_4 composites respectively during the same time duration. Furthermore, the decomposition ratios of 5 and 10% GO/Ag_3PO_4 composites were extremely fast 20 min before and noticeably slowed down 25 min after. The same result could also be concluded that 5 and 10% GO/Ag_3PO_4 composites exhibited a better photocatalytic activity, and among the catalysts 10% GO/Ag_3PO_4 composites had the best performance in photodegradation of MO under solar irradiation. Compared with the degradation under visible-light irradiation, the degradation under solar irradiation degraded more thoroughly and had a faster degradation speed and higher degradation rate.

The time-dependent absorbance of MO using 5% GO/Ag_3PO_4 photocatalyst was shown in Fig. 7. The characteristic absorption peak of MO was located at 462 nm around and with the increase of irradiation time, the intensity of the peak was decreased indicating that the concentrate of MO solution was decreased gradually, which was coincide with the dates of Figs. 5, 6.

According to the Langmuir–Hinshelwood equation: $\ln(C_t/C_0) = -kt$, the rate constants (k) of MO photodegradation using the four GO/Ag_3PO_4 photocatalyst could be calculated, as shown in Fig. 8. It could be observed that the degradation of MO by the GO/Ag_3PO_4 photocatalyst under visible-light irradiation followed the first-order kinetics reaction model and all the samples which added GO shown higher rate than pure Ag_3PO_4. Furthermore, the reactive rate constant of 5% GO/Ag_3PO_4 was 0.04396 min^{-1}, which was 14.5 times that of pure Ag_3PO_4 (0.00304 min^{-1}) under the same irradiation conditions.

Fig. 7 Absorption spectra of the MO solution taken at different degradation times using 5% GO/Ag_3PO_4 photocatalyst

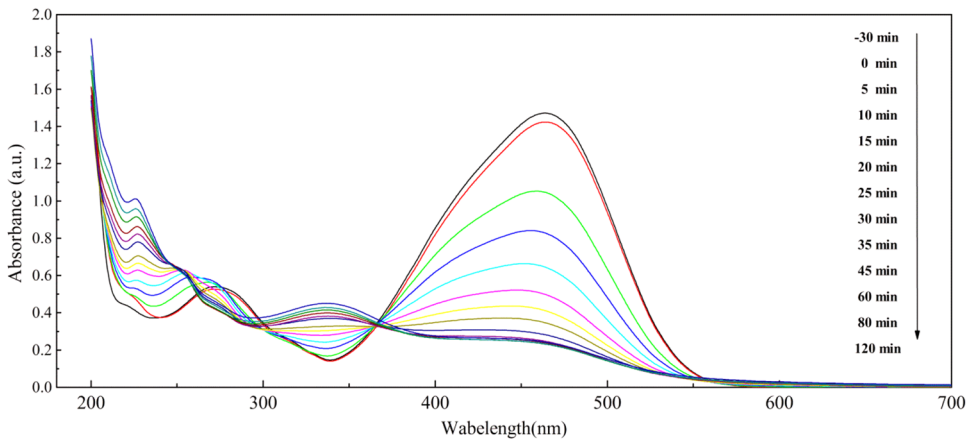

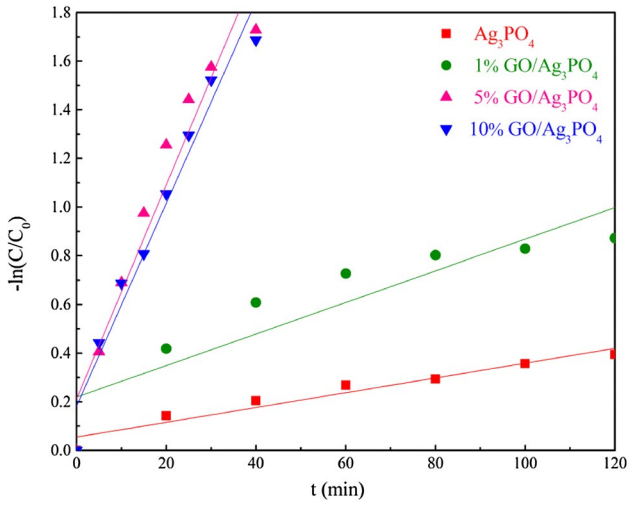

Fig. 8 Photocatalytic degradation kinetic fitting of different Ag_3PO_4 samples under 300 W Xe irradiation

4 Conclusions

In summary, a series of GO/Ag_3PO_4 nano-photocatalysts for degradation of MO was successfully synthesized by the electrostatic driving method in the present of PVP, ammonia and different content of GO, which was prepared by the modified Hummers' method. Comparing with pure Ag_3PO_4, the GO/Ag_3PO_4 photocatalysts exhibited higher photocatalytic activity and stability. According to the result of degradation, 5% GO/Ag_3PO_4 and 10% GO/Ag_3PO_4 shown the highest photocatalytic activity under visible-light irradiation and solar irradiation respectively. Furthermore, photocatalytic efficiency of 5% GO/Ag_3PO_4 was increased about 14.5 times than pure Ag_3PO_4 under visible-light irradiation. The enhancement of photocatalytic efficiency of GO/Ag_3PO_4 was strongly dependent on the involving of GO, which worked as a support to provide vast reaction locus, as well as an electron acceptor to restrain the recombination of the electron–hole pairs in Ag_3PO_4. Furthermore, GO had effectively inhibited the photocorrosion from Ag_3PO_4 to Ag and improved the stability of Ag_3PO_4, which provides a possibility of the practical application of Ag_3PO_4 in contaminant degradation. The high catalytic activity and stability of the GO/Ag_3PO_4 photocatalysts also encourage that introduce of GO is a promising way to improve the performance of photocatalysts.

References

1. R.P. Schwarzenbach, T. Egli, T.B. Hofstetter, U.V. Gunten, B. Wehrli, Annu. Rev. Environ. Resour. **35**, 109 (2010)
2. H. Tong, S. Ouyang, Y. Bi, N. Umezawa, M. Oshikiri, J. Ye, Nano-photocatalytic materials: possibilities and challenges. Adv. Mater. **24**, 229 (2012)
3. Y. Wu, M. Xu, X. Chen, S. Yang, H. Wu, J. Pan, X. Xiong, Nanoscale **8**, 440 (2016)
4. A. Fujishima, K. Honda, Nature **238**, 37 (1972)
5. F. Zuo, K. Bozhilov, R.J. Dillon, L. Wang, P. Smith, X. Zhao, C. Bardeen, P. Feng, Angew. Chem. **51**, 6223 (2012)
6. B. A. Bhanvase, T.P. Shende, S.H. Sonawane, Environ. Technol. Rev. **6**, 1 (2017)
7. S. Topcu, G. Jodhani, P.I. Gouma, Front. Mater. **3**, 1 (2016)
8. C.L. Bianchi, C. Pirola, F. Galli, M. Stucchi, S. Morandi, G. Cerrato, V. Capucci, Rsc Adv. **5**, 53419 (2015)
9. Z. Tong, Y. Dong, T. Xiao, T. Yao, Z. Jiang, Chem. Eng. J. **260**, 117 (2015)
10. J. Tian, Y. Leng, Z. Zhao, Y. Xia, Y. Sang, P. Hao, J. Zhan, M. Li, H. Liu, Nano. Energy **11**, 419 (2014)
11. Z. Yi, J. Ye, N. Kikugawa, T. Kako, S. Ouyang, H. Stuartwilliams, H. Yang, J. Cao, W. Luo, Z. Li, Nat. Mater **9**, 559 (2010)
12. D.J. Martin, G. Liu, S.J.A. Moniz, Y. Bi, A.M. Beale, J. Ye, J. Tang, Chem. Soc. Rev. **44**, 7808 (2015)
13. Q. Xiang, L. Di, T. Shen, L. Fan, Appl. Catal. B **162**, 196 (2015)
14. N. Umezawa, O. Shuxin, J. Ye, Phys. Rev. B **83**, 287 (2011)
15. H. Fan, T. Jiang, H. Li, D. Wang, L. Wang, J. Zhai, D. He, P. Wang, T. Xie, J. Phys. Chem. C **116**, 2425 (2012)
16. H. Kim, H.Y. Yoo, S. Hong, S. Lee, S. Lee, B.S. Park, H. Park, C. Lee, J. Lee, Appl. Catal. B Environ. **162**, 515 (2015)
17. Y. He, L. Zhang, B. Teng, M. Fan, Sci. Technol. **49**, 649 (2015)
18. C.N. He, W.Q. Huang, X. Liang, Y.C. Yang, B.X. Zhou, G.F. Huang, P. Peng, W.M. Liu, Sci. Rep. **6**, 22267 (2015)
19. J.M. Kahk, D.L. Sheridan, A.B. Kehoe, D.O. Scanlon, B.J. Morgan, G.W. Watson, D.J. Payne, J. Mater. Chem. A **2**, 6092 (2013)
20. M. Cao, P. Wang, Y. Ao, W. Chao, J. Hou, Q. Jin, Int. J. Hydrogen Energy **40**, 1016 (2015)
21. H. Yu, Y. Yu, J. Liu, P. Ma, Y. Wang, F. Zhang, Z. Fu, J. Mater. Chem. A **3**, 19439 (2015)
22. L. Gan, L. Xu, K. Qian, Mater. Des **109**, 354 (2016)
23. H. Xu, C. Wang, Y. Song, J. Zhu, Y. Xu, J. Yan, Y. Song, H. Li, Chem. Eng. J. **241**, 35 (2014)
24. X. Hu, Q. Zhu, X. Wang, N. Kawazoe, Y. Yang, J. Mater. Chem. A **3**, 17858 (2015)
25. X. Bai, L. Wang, R. Zong, Y. Lv, Y. Sun, Y. Zhu, Langmuir **29**, 3097 (2013)
26. L.L. Tan, W.J. Ong, S.P. Chai, B.T. Goh, A.R. Mohamed, Appl. Catal. B Environ. **179**, 160 (2015)
27. K. Dai, L. Lu, C. Liang, G. Zhu, Q. Liu, L. Geng, J. He, Dalton Trans. **44**, 7903 (2015)
28. J. Li, L. Wei, C. Yu, W. Fang, Y. Xie, W. Zhou, L. Zhu, Appl. Surf. Sci. **358**, 168 (2015)
29. H.K. Chae, D.Y. Siberiopérez, J. Kim, Y. Go, M. Eddaoudi, A.J. Matzger, M. O'Keeffe, O.M. Yaghi, Nature **427**, 523 (2004)
30. M. Minella, M. Demontis, M. Sarro, F. Sordello, P. Calza, J. Mater. Sci. **50**, 2399 (2015)
31. H. Mudila, S. Rana, M.G.H. Zaidi, J. Anal. Sci. Technol. **7**, 3 (2016)
32. W. Wan, S. Yu, F. Dong, Q. Zhang, Y. Zhou, J. Mater. Chem. A **4**, 7823 (2016)
33. A.Z. Hossein, R. Elaheh, Talanta **144**, 769 (2015)
34. Y. Liu, F. Luo, S. Liu, S. Liu, X. Lai, X. Li, Y. Lu, Y. Li, C. Hu, Z. Shi, Small **13**, 14 (2017)
35. H. Zhang, X. Lv, Y. Li, Y. Wang, J. Li, Acs Nano **4**, 380 (1936)
36. G. Chen, M. Sun, Q. Wei, Y. Zhang, B. Zhu, B. Du, J. Hazard. Mater. **244–245**, 86 (2013)
37. Y. Ao, P. Wang, C. Wang, J. Hou, J. Qian, Appl. Surf. Sci. **271**, 265 (2013)

38. X. Yang, H. Cui, Y. Li, J. Qin, R. Zhang, H. Tang, Acs Catal. **3**, 363 (2013)
39. X. Fu, F. Bei, X. Wang, S. O'Brien, J.R. Lombardi, Nanoscale **2**, 1461 (2010)
40. L. Liu, J. Liu, D.D. Sun, Catal. Sci. Technol. **2**, 2525 (2012)
41. Q. Yan, M. Xu, C. Lin, J. Hu, Y. Liu, R. Zhang, Environ. Sci. Pollut. Res. **23**, 14422 (2016)
42. Y. Wang, R. Shi, J. Lin, Y. Zhu, Appl. Catal. B **100**, 179 (2010)
43. P. Dong, Y. Wang, B. Cao, S. Xin, L. Guo, J. Zhang, F. Li, Appl. Catal. B **132–133**, 45 (2013)